Surface Electric Fields and Geomagnetically Induced Currents in the Scottish Power Grid During the 30th October 2003 Geomagnetic Storm

Alan W. P. Thomson, Allan J. McKay, Ellen Clarke and Sarah J. Reay

British Geological Survey, West Mains Road, Edinburgh, EH9 3LA, UK

Corresponding Author

Alan W P Thomson, British Geological Survey, West Mains Road, Edinburgh, EH9 3LA, UK. (awpt@bgs.ac.uk; tel: +44 131 650 0257; fax: +44 131 668 4368)

Abstract

A surface electric field model is used to estimate the UK surface *E*-field during the 30th October 2003 severe geomagnetic storm. This model is coupled with a power grid model to determine the flow of geomagnetically induced currents (GIC) through the Scottish part of the UK grid. Model data are compared with GIC measurements at four sites in the power network. During this storm measured and modelled GIC levels exceeded 40A and the surface electric field reached 5V/km at sites in the UK (compared with quiet time levels of less than 0.1 V/km). The electric field and grid models now form part of a GIC monitoring, analysis and warning software package with web interface, developed for use by the grid operator. This package also contains a daily geomagnetic activity forecast service, a solar wind shock detector, for geomagnetic storm warning, and a near real time geomagnetic data stream, for storm monitoring.

AGU Index Terms

1515 Geomagnetic induction;

2788 Magnetic storms and substorms;

5109 Magnetic and electrical properties.

7904 Geomagnetically induced currents

7934 Impacts on technological systems

Key Words

Geomagnetically induced currents; space weather; electrical power grids; transformers; geomagnetic storm; surface electric field.

1. Introduction

During geomagnetic disturbances the geoelectric field at the Earth's surface drives geomagnetically induced currents (GIC) through conductor networks, such as power grids, gas and oil pipelines. To investigate the flow of GIC in a given system we need to understand how the geoelectric field responds to a geomagnetic disturbance (e.g. Viljanen and Pirjola, 1994). However, the geoelectric field is sensitive to variations in the Earth's resistivity (e.g. Bahr, 1991). The UK landmass has a complex geological structure. In addition, shallow shelf seas surround it, with deep ocean a few hundred kilometres to the west and continental Europe nearby to the east. These factors are known to influence the electromagnetic fields observed on land (Beamish, 1985; Ritter and Banks, 1998). Gilbert (2005) has also recently highlighted the relevance of the 'coast-effect' for GIC, where the onshore electric field magnitude is enhanced considerably due to the large mismatch in the conductivities of the ocean and land. In the next section we discuss some recent developments towards an accurate three dimensional conductivity model for the UK and the neighbouring continental shelf and, in particular, we estimate the large surface electric fields that occurred during the October 2003 'Halloween' geomagnetic storm. Magnetotelluric and Geomagnetic Deep Sounding data have been used to help refine the model, particularly in the Midland Valley region of Scotland.

In the Midland Valley region there is an extensive 275kV and 400kV network of power lines and transformers. It is well known (e.g. Boteler *et al*, 1998; Bolduc, 2002; Molinski, 2002; Kappenman, 2004) that high voltage network transformers may suffer problems because of saturation due to GIC (e.g. reactive power losses, AC odd and even harmonic generation, stray magnetic flux heating) and the Scottish grid operator, Scottish Power plc, has installed GIC

monitoring equipment at four key sites in the high voltage grid. In Section 3 we describe an electrical network model of this power grid. We compare model and measured GIC data at these and other sites and discuss the accuracy of the model.

From these studies we have developed a GIC web tool and this is described in Section 4. The components of this tool are a daily three-day ahead geomagnetic activity forecast (produced from publicly available solar and geomagnetic data), a solar wind shock monitor (using near real time data from the NASA ACE spacecraft, courtesy of NOAA/SEC), a real time geomagnetic index for the UK (for monitoring storm growth and decay), and the GIC model described in Sections 2 and 3 (i.e. surface electric field and power network models). The web tool updates data and displays every ten minutes providing users with a full range of near real time data, for example to aid grid management.

We conclude in Section 5 with a summary, some observations on GIC issues, and plans for future developments.

We first review some of the other UK impacts of the severe geomagnetic storm of October 29-30 2003. This storm was notable in the UK not least because of the very high rates of change observed in the geomagnetic field. The storm followed the eruption of two solar flares from the same active region (NOAA 10486) on the 28th and 29th October 2003. The first, an X17 X-ray flare, was one of the largest recorded events. The second flare, an X10, erupted 33 hours later. Both flares had associated Earth-directed coronal mass ejections. The first CME impacted the Earth's magnetosphere on 29th October 2003 after a travel time of around 19 hours. This caused

large variations in the Earth's magnetic field. At Lerwick observatory in Shetland, to the north of Scotland, the magnetic compass direction varied between 0° and 7° west of north during the storm. The disturbance continued for 20 hours and had started to decline when the second CME arrived on 30th October 2003. Again the magnetic field variations were significant, although this time the largest variations were seen further south. Remarkably, at Eskdalemuir observatory (situated in Southern Scotland) the magnetic compass direction changed by over 5° in only 6 minutes at around 21:20 UT (see Figure 1). The aurora borealis is usually visible only at high UK latitudes, towards the north of Scotland. However the magnitude of these magnetic storms gave rise to two nights of spectacular auroral displays throughout the UK.

Importantly, Eskdalemuir observatory lies within the Scottish Border region, less than 100km from a major east-west 400kV power line (Figure 2), with a termination at the Strathaven substation (STHA in Figure 2). GIC measuring equipment operated by Scottish Power at Strathaven recorded 42A flowing to Earth in a single transformer (three-times-phase) around the peak of the storm (Figure 3). Scottish Power engineers suggested that 42A, if sustained, would definitely have caused transformer problems (T. Cumming, Scottish Power, personal communication). However, the interplanetary magnetic field remained northward for much of the time during the storm, inhibiting reconnection on the dayside magnetopause, and this probably contributed to the few actual problems observed on the network (see also Simpson, 2003). Transformer heating (gas production) and voltage fluctuations were observed but were regarded as being at manageable levels. Post-event considerations by engineers now suggest that a threshold level of GIC of about 25 A constitutes an approximate 'concern threshold' for the Scottish Power grid operators, transmission and transformer engineers, with this particular

system as it now exists. This power grid, as with many others worldwide, is in a more or less constant state of evolution and this 'concern threshold' will undoubtedly change with time.

Beyond the UK a GIC related power outage in Malmö, Sweden, occurred at approximately 20:07 UT and lasted for about forty minutes (Lundstedt, 2004). The geomagnetic latitude of Malmö is comparable to that of central Scotland. Indeed, GIC in the Scottish Power grid were also enhanced at this time, with GIC at NEIL reaching approximately 25 A, during intensification of a western electrojet. We note that the peak GIC observed on 30th October 2003 exceeds known GIC in the UK in previous storms (Beamish *et al*, 2002; Erinmez *et al*, 2002). Other technological effects, such as satellite, aviation and ground-based anomalies, of the 28th-30th October space weather event, and those that occurred throughout late October and early November 2003 (the so-called Halloween epoch events) have been reviewed elsewhere in detail. For example, Webb and Allen (2004) highlight that a number of earth orbiting satellites suffered spontaneous Central Processor Unit resets and memory errors, and that the Federal Aviation Authority took the unprecedented step of issuing an alert to airline passengers regarding the possibility of high radiation doses. Similarly, Barbieri and Mahmot (2004) detail both spacecraft anomalies and the operational effects of the space weather events. These Halloween events have also been used to assess both the performance of real-time shock arrival production schemes and forecast accuracy (Dryer *et al*, 2004; Oler, 2004).

2. Modelling the Surface Electric Field in the UK

Beamish *et al* (2002) described a surface electric field model for the UK, Ireland and surrounding seas, based on a conductivity model comprising a six-block tectonic terrane

structure for the UK crustal landmass, to a 30 km depth, on top of a radially varying conductivity model of the lithosphere and upper mantle, down to 1000 km. This model also included the conductivity of the surrounding shelf seas (~200 m depth of water). The UK and Ireland was modelled on a 20 km square grid and electric fields were estimated for plane wave inducing fields using finite difference equations (e.g. Mackie *et al*, 1994). Beamish *et al* (2002) considered two fixed periods of field variation, of 10 and 30 minutes, appropriate for longer period GIC studies. They concluded that, for the long period variations they considered, the crustal structure of the UK serves to redistribute the amplitude and phase of the secondary electric field induced in both the crust and mantle as result of the primary electromagnetic fields of ionospheric and magnetospheric origin. Large surface *E*-field enhancements at the terrane boundaries and at the coast were noted. However, Beamish *et al* (2002) were forced to use a seawater resistivity that was sixteen times too large, to ensure that the minimum skin depth encountered in the model was greater than their choice of numerical grid spacing, which is a normal requirement of most electromagnetic modelling algorithms. They highlighted that this effectively reduced the conductivity contrast between the sea and the land, which in turn reduced the amplitude of the surface electric field due to the lateral contrast in conductivity. In addition, while the Mackie *et al* (1994) algorithm allows fully 3D variations of resistivity, the primary electromagnetic fields were limited to plane-waves.

McKay (2004) circumvented these drawbacks by modelling the electric field using the thin-sheet approximation (e.g. Weaver, 1982) and the modelling algorithm of Vasseur and Weidelt (1977). Thin-sheet modelling is particularly suited to studying geomagnetic induction where lateral variations in conductivity occur in a thin sheet at, or close to, the surface of the Earth. In

addition, a thin-sheet algorithm provides computational advantages. Only the horizontal components of the electric field need be computed and an arbitrary primary magnetic field may be considered. A full description of the construction of the UK thin-sheet model is given in McKay (2004) and in a paper currently in preparation. Therefore only a brief description is given here. McKay (2004) developed the model by incorporating Geomagnetic Deep Sounding (GDS) and Magnetotelluric (MT) data for the Midland Valley (MV), Southern Upland (SU), and the northern portion of the Concealed Caledonides (CC) terranes and by properly accounting for the high seawater conductivity, which was underestimated in the Beamish *et al* (2002) study. The improved model includes detailed bathymetry data for the shelf seas and Atlantic Ocean and uses a finer grid scale, at 10km. Figure 4 shows the original tectonic structure adopted for the British Isles by Beamish *et al* (2002) and the new (depth-integrated) conductance model of the ocean and shelf-seas of McKay (2004), which assumes a sea-water resistivity of 0.25 Ohm m. McKay represents the top-most sheet of the crustal structure of Beamish *et al* (2002) as a laterally varying conductance map (as in Figure 4), together with new crustal scale on-shore conductivity variations in the MV, SU and CC regions, chosen to enhance the agreement with measured MT and GDS data. Underlying this new thin layer McKay retains the 1D model of Beamish *et al* (2002).

The relevance of a 3D model is emphasised by data in McKay (2004) that shows the distorting effect of a major terrane boundary on measured GIC data at the TORN site (see Figures 2 and 4) as well as local crustal effects at STHA. Significant regional conductance contrasts are also implied by the observed azimuthal variations when telluric responses calculated from MT measurements are displayed in the form of ‘telluric vectors’. Telluric vectors are the electric

fields associated with a unit magnetic induction linearly polarised in a north-south and east-west direction (Bahr, 1991). A common problem in the interpretation of MT measurements is caused by the electrostatic (often referred to as galvanic) distortion of the electric field due to conductivity anomalies which are much smaller than the true electromagnetic skin-depth. This causes the well-known 'static-shift' of the MT parameter apparent resistivity, whose magnitude is shifted up or down by an unknown amount in a frequency independent manner. When plotted on a geographical map the distortion of the telluric vectors is easily recognised: the telluric vectors of MT sites that are closely spaced (e.g. the site spacing is smaller than the estimated skin-depth) have magnitudes and azimuths that are inconsistent with neighbouring sites. The regional telluric responses were therefore recovered using the method of Smith (1995). Regional responses determined using such methods account for the angular distortion of the electric field but it is not possible to quantify uniquely the effect on the magnitude of the electric field without additional information. Figure 5 shows the telluric responses of model and measured data (corrected for distortion) in the MV-SU region for an east-west or north-south inducing field at 750s period (McKay, 2004). This is roughly in the middle of the range of periods relevant to GIC studies (i.e. few seconds to ~30 minutes or so). In order to extract model telluric vectors at the MT sites the electric field model output was interpolated onto a 1 km grid. Clearly there is a strong azimuthal consistency between measured and modelled data in Figure 5, with less consistency in the magnitude of the vector responses. The measured data show large local variations in amplitude whereas the model data appear more locally uniform. The measured telluric vectors have amplitudes up to 6.9 mV/km per unit (nT) inducing field while the model data are no more than 1.1 mV/km. The large magnitude of the measured telluric responses is correlated over distances of approximately 10-20 km. This gives an indication of the spatial scale

of electric field distortion in this region at a period of 750 s. This spatial-scale is similar to the current node spacing (10 km) of the electric field model. A smaller node spacing would be required to investigate the possible effects of such large amplitude distortions.

Based on these model developments, Figure 6 presents an estimate of the surface electric field across the UK and Ireland during the peak of the 30th October 2003 magnetic storm, at 21:20 UT. The amplitude of the horizontal inducing field is that measured at Eskdalemuir observatory, at 1400 nT and oriented slightly east of south at that time. We have assumed a driving period of six minutes on the basis of the north field component profile around 21:20 UT. A north-south gradient in the amplitude of the primary inducing field was also imposed on the basis that the amplitude of the geomagnetic disturbance in the northern region of the UK was two to three times that in the southern region. This gradient was determined from the measurements from the three UK observatories, from Lerwick in the north of Scotland to Hartland in the south of England.

The peak magnitude of surface fields in the UK, typically increasing towards the more resistive north of the country, was over 5 V/km, in comparison with typical quiet levels of under 0.1 V/km. There is also much regional structure in the MV-SU region and strong coastal contrasts. Of course Figure 6 represents no more than a snapshot of possible conditions during a period of rapid change, both in amplitude, phase and driving frequency. It may also underestimate actual field strengths and local *E*-field azimuths in the MV-SU region, based on the evidence of Figure 5. It does however provide some good corroboration, in the form of GIC estimates, as is seen in the next section.

3. GIC in the UK Grid

A transfer function (TF) method has been applied to correlate GIC data recorded at the Scottish Power monitoring sites shown in Figure 2 and simultaneous magnetic measurements at Eskdalemuir observatory (based on a method described in McKay, 2004). The TF for each site relates the two data sets in the frequency domain. Although the TF for each site was derived using data during various storms in 2000 and 2001, it can be seen in Figure 7 that the TF method does an adequate job of reproducing the measured data during the October 2003 severe storm, even though changes in grid configuration in the intervening time were expected to degrade the model. Probably the most significant change in the network since the year 2000 is that STHA and TORN are now connected directly by a 130 km long 400 kV circuit. Previously this connection was broken down into 75 and 55 km segments rated at 275 and 400 kV respectively. The previous connection therefore consisted of a 400-275 kV transformer. However, amplitudes are still relatively well reproduced, as is much of the time variation.

Interestingly some of the longer period signals (e.g. HUNT at around 20:15 UT) are apparently of the 'wrong' sign. This may be a consequence of the greater uncertainty in the accuracy of the TF coefficients at the longest periods (McKay, 2004). Where a dominant signal is found at such periods, then the sign may appear reversed if it is of small amplitude, as in parts of Figure 7. (In the TF model used here, periods up to about 17 minutes long are considered, though this can be varied. TF models formed from longer data-vectors may improve spectral resolution at longer periods but are less useful for near real time work, as in Section 5.) The Neilston (NEIL) and Strathaven (STHA) sites are those where most substation development work has probably been undertaken since 2000, but these are arguably not poorer than elsewhere. The TF-estimated data

for the 29th October 2003 event prove equally as accurate as those in Figure 7 and have helped interpret the likely GIC variations during periods in that day when measured data were actually unavailable. However the estimated peak GIC do not exceed those on the 30th October, so are not reproduced here.

A Scottish grid electrical network model, constructed following the work of Beamish *et al* (2002) and subsequently further developed by McKay (2004), has been used to estimate peak GIC flows during 29th-30th October 2003. This model follows the methodology of Lehtinen and Pirjola (1985) and Viljanen and Pirjola (1994) and the relevant portion is shown in Figure 2. Lumped resistances in the model represent the UK grid to the south in England and Wales. The network admittance matrix for the 275kV and 400kV high voltage (HV) network is formulated with reference to the Scottish Power plc "Seven Year Transmission Statement". We assume straight-line connections between nodes in the transmission network but use the actual line length in order to calculate the power line resistance. The earthing impedance matrix for the 118 HV transformers in the grid at year 2000, used in this paper, incorporates the resistance of the transformer windings and the earthing system of 'grid' or inductive transformers as well as the system of autotransformers. Transformer modelling follows Mäkinen (1993), with the addition of virtual nodes and adjustment of the earthing and network admittance matrices, where necessary. Data for these are also available from the transmission statement. For simplicity, we assume that each transformer is independently earthed. For example, at one particular site (Strathaven) there are two transformers rated at 400-275 kV and 275-33 kV. However, these transformers are located in different places, and are each connected to different earth systems.

We assume, that the GIC in one neutral does not cause a potential shift in the other i.e. the impedance matrix is diagonal.

The model may be incomplete in places. For example, as is discussed in McKay (2004), the neglect of the substantial (if short line-length) 132 kV network can affect the way in which individual transformers are modelled. Indeed, autotransformers can make it difficult to predict the location, size and polarity of GIC in a network because different parts of the network are in direct electrical contact (Koen, 2002). Therefore, we are neglecting paths along which GIC may flow. This is not usually considered a serious concern because, in general, transmission lines become shorter and their electric resistance increases as the system voltage decreases. However, McKay (2004) illustrated, by considering the ratio of the transmission line-length to its resistance (to which transmission line GIC magnitude will be proportional), that neglecting the 132 kV network may not be well justified for at least some GIC sites. For example, the mean ratio of line length to resistance of all connections to the four Scottish Power monitoring sites for the 400, 275 and 132 kV circuits is 35±9, 27±1 and 18±11 [km/Ohm] respectively. Note that these values are for a single transmission line phase. In addition, the 275-132 kV auto-transformer common winding resistances are smaller than that of the 400-275 kV auto-transformers. We also think that the assumption of straight-line node connections may also be questionable where there is significant *E*-field lateral variation (e.g. as in Figures 5 and 6).

Figure 8 shows a snapshot of the grid model output just before 21:20 UT on the 30th October. There is a clear east-west trend in the sign of GIC (i.e. generally, if not exclusively, 'in' to the grid on the west coast and 'out' of the grid on the east coast) but with a wide variation in GIC

amplitude. It is notable from Figure 8 that there may be larger estimated GIC at other sites in the power grid, in comparison to the monitoring sites, and these other sites are generally close to both west and east coasts.

That differences in the peak times of measured GIC variations can be important is emphasised by the GIC time series at the permanent measurement sites shown in Figure 9. We show for comparison GIC model calculations. The thin-sheet model remains computationally unwieldy for near real time calculation of GIC time series. Therefore we show results from model calculations using a 1D geoelectric field model of the region extracted from the thin-sheet model, and geomagnetic data from Eskdalemuir. Figure 9 shows the measured and model data. For example, at STHA the peak current is about –42 A just before 21:20 UT. At that time the model output is only –20 A (see also Figure 7), although it subsequently goes below –40 A within one minute. In Figure 9 there are a number of other observations that can be made. At HUNT, the model GIC is arguably of the 'wrong' sign in places and the dominant frequencies are not so well reproduced toward the end of the time frame. At NEIL the measured time series is reasonably well tracked and peak amplitudes (if not sign) are representative of the measured data. At TORN the measured GIC are generally smoother and of lower amplitude but this is not reflected in the modelled GIC. This highlights one drawback of using a 1D electric field model: each GIC monitoring site has distinct amplitude and phase characteristics that reflect the driving electric field sampled by each site. However, the amplitude and phase response of the modelled 1D electric field, at any given frequency, is uniform throughout the region. In practice, small spatial details of the geoelectric field are unimportant, because we integrate the geoelectric field along the path of transmission lines and therefore smooth local variations. However, in using a single

1D model we neglect variations of the geoelectric field due to lateral changes in conductivity, which are of comparable scale to the length of the transmission lines.

We should note that the total estimated transformer neutral GIC at each site is given, whereas the measured GIC are taken from one single transformer. Thus, at NEIL for example, the model GIC are the sum of the calculated GIC in each of the three transformer neutrals included in the Scottish Power grid model. Only the total GIC are determined because we believe that our electrical model of the major sites, with complicated grounding arrangements amongst transformers (of which NEIL and STHA are two such sites) is probably still incomplete. Overall there is a close similarity between the model data for the three western sites, but this is less true of the measured data, emphasising the significance of the detail required of the grid and/or conductivity models.

The difference, in Amps, between measured GIC and GIC calculated using both the numerical and transfer function models is shown in Figure 10. These differences were calculated on a point by point basis i.e. no smoothing or averaging of the data has been carried out. Qualitatively, we note that the Transfer Function model currently performs better than the numerical model at three sites (HUNT, NEIL and TORN) but at STHA the performance of both methods is almost comparable. At all sites the difference between the measured GIC and GIC modelled using the numerical model is rather large and in some cases approaches the size of the largest measured GIC. However, it is important to recognise that such a comparison does not account for any phase difference between the measured and modelled GIC. For example, the modelled GIC at STHA lag the measured GIC by approximately 50 s. By aligning the peaks of maximum GIC we

find that the largest and most obvious differences can be reduced by approximately 50 %, but that the overall root mean square difference between measured and modelled GIC is largely unaffected. In any case, the overlain plots (Figures 7 and 9) show that both methods provide an accurate sense of the times at which the largest GIC occur e.g. to within a minute or so of measured GIC enhancements. Further work is required in order to refine the numerical model and one possible strategy is to attempt to use an inverse method to go from the measured GIC and geomagnetic data to a conductivity model.

Figure 11 summarises the model accuracy at various levels of confidence, obtained by a quantile-quantile analysis of the (model-measured) residuals during the two days of the storm. At the 95% confidence level, the numerical network model analysis proves typically between 2-3 times less certain than the TF model. The exception to this is at STHA, where the uncertainties are similar. This could be due to a number of reasons such as a particular result of the grid configuration and higher associated confidence in the grid model and its electrical parameters at that location or, STHA's relative distance from the coast. However the most likely explanation is that the STHA TF is poorly resolved by the available data, i.e. the confidence intervals are wider than they would be if more data had been available for its construction. Certainly the STHA TF estimated error is twice that typical at the other sites, thus statistical confidence in the TF estimate is decreased. Estimating the errors of the GIC data calculated using the numerical electric field model also permits assessment of the performance of the simpler 1D model in calculating GIC in both a practical and scientific sense. For example, it is interesting to note that for the numerical model the estimated errors tend be larger at those sites on the edges of the network, and close to the coast, than those located inland and within the network. This may

indicate that the 1D assumption is less well satisfied at these sites as the coastline provides a major crustal-scale lateral conductivity contrast because sea-water is much more conductive than most geological materials. Therefore, large electric field enhancements, in comparison to a 1D model, occur near the coastline (e.g. Beamish *et al*, 2002).

4. A Web Based GIC Warning and Monitoring System

In collaboration with Scottish Power plc and supported by an ESA grant through the 'Space Weather Pilot Project' scheme we have developed a web-based GIC monitoring and analysis tool for the Scottish power grid. Figure 12 shows the front page of this password-protected tool. (A public access version is under development that contains a subset of the full near real time data range, for education and demonstration purposes: http://www.geomag.bgs.ac.uk/gicpublic.) There are four 'button' options on the front page, linking to 1) real-time geomagnetic data, in the form of hourly standard deviations (the *HSD* index described in Beamish *et al*, 2002), 2) the current three day British Geological Survey geomagnetic activity forecast, 3) a list of the most recent solar wind shocks and 4) estimated real time GIC flowing in the grid at all transformer earth points.

All data and web pages are updated every 10 minutes. The tool is deliberately simple, with limited options, primarily for clarity and ease of use. For each link (i.e. button) there is some brief background information on the data being displayed as well as accuracy statistics and an email contact in the event of a query, request or data error. Text versions of the main data streams can also be downloaded. Each button changes to red to signify that a significant event has taken place or some warning threshold has been exceeded, or blinks yellow to indicate that

basic data have been recently updated. Currently we use an *HSD* threshold of 30 nT at Eskdalemuir (equivalent to the local minor storm threshold), an estimated GIC in excess of 3 A (set at a deliberately low level to indicate rising conditions), an updated forecast in the last 60 minutes, and a shock detected in the last 60 minutes, to switch on each of these flashing buttons. The flashing stops automatically after one hour.

Figure 13 shows one display available through the tool. This portrays estimated GIC in the high voltage grid network, as determined from the grid and electric field models. It also shows a single, higher accuracy, TF-estimated GIC time series with 95% confidence limits, for any one of the four permanent monitoring stations, selected by moving the mouse across the power grid map.

Scottish Power has routinely used the *HSD* index since 1999 to monitor UK geomagnetic variations and to alert grid control to the onset of high geomagnetic activity and hence raised GIC. In the web-based system the user can browse the last week of activity at high or low time resolution. Geomagnetic activity forecasts are those of likely global conditions over the next three days, with relevant local interpretation for the UK where possible. Individual forecasters make forecasts, analysing public domain space weather data. The forecast can be backed up by daytime telephone consultation and effectively provides a ‘look ahead’ service for Scottish Power that helps grid management and operation, particularly in the event of a forecast of high geomagnetic activity.

The shock monitor algorithm uses two simple algorithms applied to five-minute smoothed ACE solar wind data: a simple threshold of the solar wind data, and the wavelet-transformed data (to improve the signal to noise ratio). Currently we declare candidate shocks on a positive output

from either of these methods. System tests, using the SOHO shock catalogue for 2001 (obtained from http://umtof.umd.edu/pm/) and the list of Mozer and Briggs (2003), demonstrate that the probability of shock detection (POD) rises along with the probability of false detection (POFD). Currently we have set thresholds to attain a POD of about 0.3. This provides a POFD that is equivalent to about one false alarm per month. In practise we judge that the shocks that are missed by the system are those that are associated with less significant geomagnetic activity. In the 'fall back' mode, used when only the total IMF is available (e.g. if the ACE 'SWEPAM' instrument is temporarily disabled by a very high speed interplanetary coronal mass ejection), the POFD rises to one false alarm per week, for a similar level of POD.

5. Summary and Discussion

The surface electric field and GIC models both provide a reasonable fit to data though they also show aspects that need to be improved, not least in the appearance of 'wrong sign' GIC at some substations. These differences will be investigated. The effect of more detailed ionospheric fields (rather than simple planar currents), and the sensitivity of the model output to transformer and line electrical parameters, require investigation and may prove important. It has also been shown (McKay, 2004) that the extensive 132 kV grid system may not be irrelevant, partly on the basis of estimates of the system electrical resistance, as had been previously believed. This network provides many other paths for GIC to flow, and provides alternative connections across the higher voltage system. The electric field model has reached a level of maturity (Beamish *et al*, 1998; Beamish *et al*, 2002; McKay, 2004) that is difficult to take forward, without additional measurement databases for comparison, although different modelling methodologies may provide other ways to construct conductance models (e.g. Wang and Lilley, 1999). A finer scale

conductivity model might be desirable in some places, i.e. less than the 10 km grid used at present, but for most practical purposes this should be sufficient. Future efforts will concentrate on refining the grid network model. In fact, we find that the output from a simpler 1D conductivity model is almost as good as the 3D model output during most geomagnetic storm events so far examined (e.g. the small range of *E*-field azimuths in Figure 6) insofar as the 1D model calculations highlight when the largest GIC occur and provide a bounded estimate of GIC magnitude. Therefore the 1D modelling is considered adequate for most practical (i.e. user) purposes. Therefore we do not propose to develop the 3D model further at this time. However, it should be remembered that in order to fully understand the amplitude and phase characteristics of GIC data a 3D model is essential.

GIC risk to equipment in power grids may be circumvented by technical or operational means but the trend to increased interconnections between national power grids, as well as the increasing use of higher voltage, lower resistance systems, means that the risk cannot yet be described as ‘solved’. Indeed pan-continental studies of GIC risk are probably becoming increasingly relevant. Problems due to GIC in one country can have impact elsewhere, for example in nations reliant on power imports, even by DC submarine links. In determining GIC risk to power grids during times of severe geomagnetic storms, the use of models such as those presented in this paper will be necessary. A key requirement, as has been discussed here, will be the need to properly quantify model accuracy against measured data and to continue to prompt the power industry to continue such measurements.

Further improvements to the GIC web tool are planned. There is a clear user need for a predictive element of changes in GIC levels in power grids (e.g. Erinmez *et al*, 2002). Predictions of geomagnetic variations, for example directly from solar wind data by non-linear means (e.g. Wu and Lundstedt, 1996) are one way of adding lead-time to warnings of increasing GIC. The issue of the accuracy of such predictions will have to be addressed, however, and the effective furthest 'forecast horizon' will need to be determined. Otherwise it is expected that the tool will evolve in response to the grid operator's demands.

Acknowledgements

This paper would not have been possible without the data, advice and assistance of David McMenemy, Tom Cumming, Tom Breckenridge and Ian Frame of Scottish Power plc. The web tool was developed with support from Scottish Power and the European Space Agency 'Space Weather Pilot Project' program (http://www.estec.esa.nl/wmwww/wma/spweather/). The near real time availability of data from the NASA ACE spacecraft, from the UK magnetic observatory network and the modelling support of Ari Viljanen of the Finnish Meteorological Institute are all gratefully acknowledged. We would also like to acknowledge forecasting support, previous GIC analysis and contributions to the web tool from Orsi Baillie of the British Geological Survey. The comments and suggestions provided by two anonymous referees improved this paper considerably and their contribution is gratefully acknowledged. This paper is published by permission of the Director, British Geological Survey (NERC).

References

Bahr, K. (1991), Geological noise in magnetotelluric data: a classification of distortion types. *Phys. Earth Planet. Inter.*, *66*, 24-38.

Barbieri, L. P., and R. E. Mahmot (2004), October - November 2003's space weather and operation lessons learned, Space Weather, 2, S09002, doi:10.1029/2004SW000064, 15 pp.

Beamish, D. (1985), The frequency characteristics of anomalous vertical fields observed in the British Isles. *J. Geophys ,57*, 207-216.

Beamish, D. (1998), GIC risk assessment for NGC: electric fields induced in and around Britain. *Brit. Geol. Surv. Tech. Rep. WE/98/32C*, British Geological Survey, Edinburgh.

Beamish, D., Clark, T.D.G, Clarke, E. and Thomson, A.W.P. (2002), Geomagnetically induced currents in the UK: geomagnetic variations and surface electric fields, *J. Atmos. Sol. Terr. Phys*., *64*, 1779-1792.

Bolduc, L. (2002), GIC observations and studies in the Hydro Quebec power system. *J. Atmos. Sol. Tess. Phys*., *64*, 1793-1802.

Boteler, D. H., Pirjola, R. J. and Nevanlinna, H. (1998), The effects of geomagnetic disturbances on electrical systems at the earth's surface. *Adv. Space Res*., *22*, 17-28.

Boteler, D.H., Pirjola, R. and Trichtchenko, L. (2002), On calculating the electric and magnetic fields produced in technological systems at the Earth's surface by a "wide" electrojet. *J. Atmos. Sol. Terr. Phys*, *62*, 1311-1315.

Dryer, M., Z. Smith, C. D. Fry, W. Sun, C. S. Deehr, and S.-I. Akasofu (2004), Real-time shock arrival predictions during the "Halloween 2003 epoch", Space Weather, 2, S09001, doi:10.1029/2004SW000087, 10 pp.

Erinmez, I.A., Kappenmann, J.G. and Radasky, W.A. (2002), Management of the geomagnetically induced current risks on the national grid company's electric power transmission system, *J. Atmos. Sol. Terr. Phys*., *64*, 743-756.

Gilbert, J. L. (2005), Modelling the effect of the ocean-land interface on induced electric fields during geomagnetic storms, *Space Weather*, 3, S04A03, doi:10.1029/2004SW000120.

Kappenman, J. G. (2004), The evolving vulnerability of electric power grids. *Space Weather*, 2(1).

Koen, J. (2002), Geomagnetically induced currents in the South African electricity transmission network. PhD thesis, University of Cape Town, South Africa, April 2002.

Lehtinen, M. and Pirjola, R. (1985), Currents produced in earthed conductor networks by geomagnetically induced electric fields. *Ann. Geophys*., *3*, 479-484.

Lundstedt, H. (2004), The Sun, Space Weather and GIC effects in Sweden, COSPAR Assembly, Paper Number PSW1-0013-04.

Mackie, R. L., Smith, J. T. and Madden, T. R. (1994), Three-dimensional electromagnetic modelling using finite difference equations: the magnetotelluric example. *Rad. Sci*., *29*, 923-935.

Mäkinen, T. (1993), Geomagnetically Induced Currents in the Finnish power transmission system. MSc Thesis, Geophysical Publications, No. 32, Finnish Meteorological Institute.

McKay, A (2004), Geoelectric fields and geomagnetically induced currents in the United Kingdom. PhD Thesis, University of Edinburgh, Scotland, January 2004 http://hdl.handle.net/1842/639.

Molinski, T. S. (2002), Why utilities respect geomagnetically induced currents, *J. Atm. Solar-Terr. Phys*., 64, 16, 1765-1778.

Mozer, J.B., and Briggs, W.M. (2003), Skill in real-time solar wind shock forecasts. *J. Geophysical Research: Space Physics*, *108*(A6), p.1-9, doi:10.1029/2003JA009827.

Oler, C. (2004), Prediction performance of space weather forecast centers following the extreme events of October and November 2003, Space Weather, 2, S08001, doi:10.1029/2004SW000076, 12 pp.

Ritter, P. and Banks, R.J. (1998), Separation of local and regional information in distorted GDS response functions by hypothetical event analysis. *Geophys. J. Int.*, *135*, 923-942.

Simpson, S. (2003), Massive solar storms inflict little damage on Earth, *Space Weather*, 1, 1012, doi: 10.1029/2003SW000042.

Smith, J. T. (1995), Understanding telluric distortion matrices. *Geophys. J. Int*., *122*, 219-226.

Vasseur, G., and Weidelt, P. (1977), Bimodal electromagnetic induction in non-uniform thin-sheets with an application to the northern Pyrenean induction anomaly. *Geophys. J. R.* Astr. Soc, *51*, 669-690.

Viljanen, A. and Pirjola, R. (1994), Geomagnetically induced currents in the Finnish high-voltage power system - a geophysical review. *Surv. Geophys*., *15*, 383-408.

Wang, L. J. and Lilley, F. E. M. (1999), Inversion of magnetometer array data by thin-sheet modelling. *Geophys. J. Int*., *137*, 128-138.

Weaver, J.T. (1982), Regional induction in Scotland: an example of three-dimensional numerical modelling using the thin-sheet approximation. *Phys. Earth Planet. Inter*., *26*, 161-180.

Webb, D. F., and J. H. Allen (2004), Spacecraft and Ground Anomalies Related to the October-November 2003 Solar Activity, Space Weather, 2, S03008, doi:10.1029/2004SW000075, 1, 3, 6-8.

Wu, J-G., and Lundstedt, H. (1996), Prediction of geomagnetic storms from solar wind data using Elman recurrent neural networks, *Geophys. Res. Lett*., *23*, 319.

Figure Captions

Figure 1. Geomagnetic declination variations (one second samples) during the storm of 30th October 2003 measured at Lerwick, Eskdalemuir and Hartland observatories in the UK.

Figure 2. The 275 kV (solid line) and 400kV (dashed line) power network of central Scotland in 2000 and the positions of the Eskdalemuir geomagnetic observatory (star) and the four permanent GIC monitoring sites (large circles). The most significant change in the network since the year 2000 is that STHA and TORN are now connected directly by a 130 km long 400 kV circuit.

Figure 3. Measured GIC and field rates of change at Eskdalemuir for 30th October 2003. Data are shown at 1-second resolution. (Comparable data for the 29th October 2003 show numerous gaps in the GIC record.)

Figure 4. The tectonic structure of the British Isles (left) as simplified and used by Beamish *et al* (2002). The conductance (S) of the shelf seas and ocean is shown (right). This conductance is presented to the model as a thin surface layer atop the crustal model of Beamish *et al* (2002). For plotting purposes the maximum conductance has been limited to 2000S; in the deep Atlantic Ocean to the west the conductance reaches approximately15,000S. Onshore, the conductance of the thin sheet is 25S, except for a regional variation within the Midland Valley, Southern Uplands and the northern region of the Concealed Caledonides. Data taken from McKay (2004).

Figure 5. Telluric vectors of the scaled regional telluric response (top), from McKay (2004), at measurement sites across Scotland and Northern England. Model telluric vectors are shown below, for the same locations. Data on left (right) are for an east-west (north-south) inducing field.

Figure 6. The surface electric field in the box shown in Figure 4 at 21:20 UT on 30th October 2003. Colour denotes *E*-field amplitude (see scale bar) in V/km. Small arrows denote the local field direction. The inset shows the regional *E*-field direction for a simpler 1D conductivity model, as well as the direction of the 360s period external magnetic field controlling induction at that time.

Figure 7. Transfer function model (grey lines) for the four permanent measurement sites, compared with measured data (black) for October 30th 2003. One-second measurements are used, with the longest transfer function wavelength less than about 17 minutes.

Figure 8. Estimated GIC from the grid network model of the Scottish Power grid, coupled with the surface electric field model of Figure 6 at the peak of the storm at 21:20 UT. Circle shade denotes GIC flowing to/from earth (dark/light) and the arrows denote the instantaneous field directions (*E*-field for a 1D conductivity model). Amplitudes are proportional to spot size, with 40A shown to scale. In order to show one value at each substation location the sum of all GIC at that site are given for clarity. White spots show the locations of the permanent GIC measurement sites.

Figure 9. Time series of model and measured GIC at the Hunterston (HUNT), Neilston (NEIL) Strathaven (STHA) and Torness (TORN) sites between 20:00 UT and 23:00 UT on the 30th October 2003. Total site GIC model flows are shown.

Figure 10. The point difference between GIC calculated using the numerical (black line) and transfer function (grey line) models between 20:00 UT and 23:00 UT on the 30th October 2003.

Figure 11. The GIC numerical (NUM) network model accuracy, based on quantile-quantile plots of residuals (in Amps) and shown at different levels of significance. Transfer

function (TF) data are also given, for comparison, at the 95% confidence level in the fourth numerical column.

Figure 12. The front page of the web based data delivery system. The page is password protected.

Figure 13. *Left*: Maximum GIC estimated in the grid in the hour prior to 22:00 UT on the 30th October 2003 (shown as a geographic map here rather than via the alternative option of a schematic layout of transformer earth points). *Right*: GIC time series for the four individual substations can be displayed, together with 95% confidence limits on the estimated current flow. The time series data are obtained from either the *E*-field and network model or (as here) from a transfer function model.

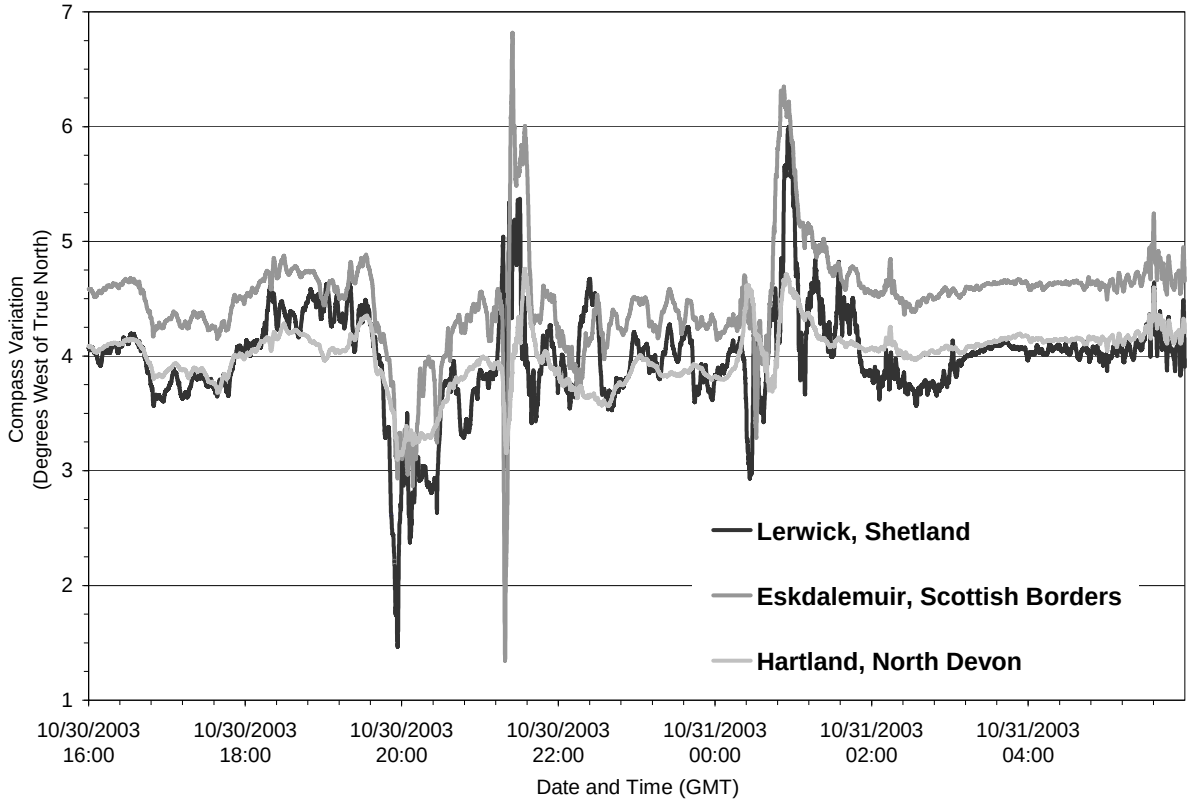

Figure 1. Geomagnetic declination variations (one second samples) during the storm of 30th October 2003 measured at Lerwick, Eskdalemuir and Hartland observatories in the UK.

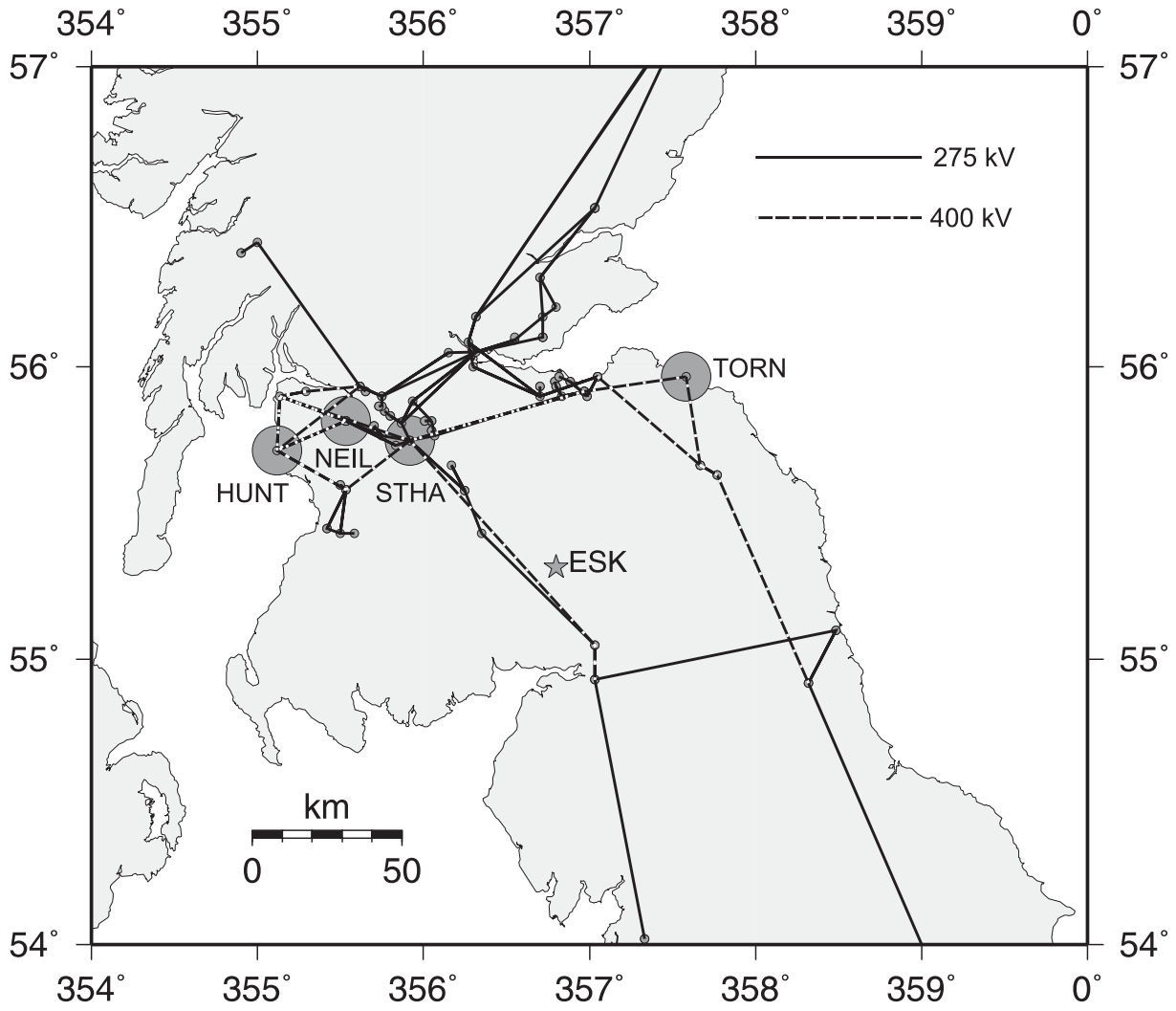

Figure 2. The 275 kV (solid line) and 400kV (dashed line) power network of central Scotland in 2000 and the positions of the Eskdalemuir geomagnetic observatory (star) and the four permanent GIC monitoring sites (large circles). The most significant change in the network since the year 2000 is that STHA and TORN are now connected directly by a 130 km long 400 kV circuit.

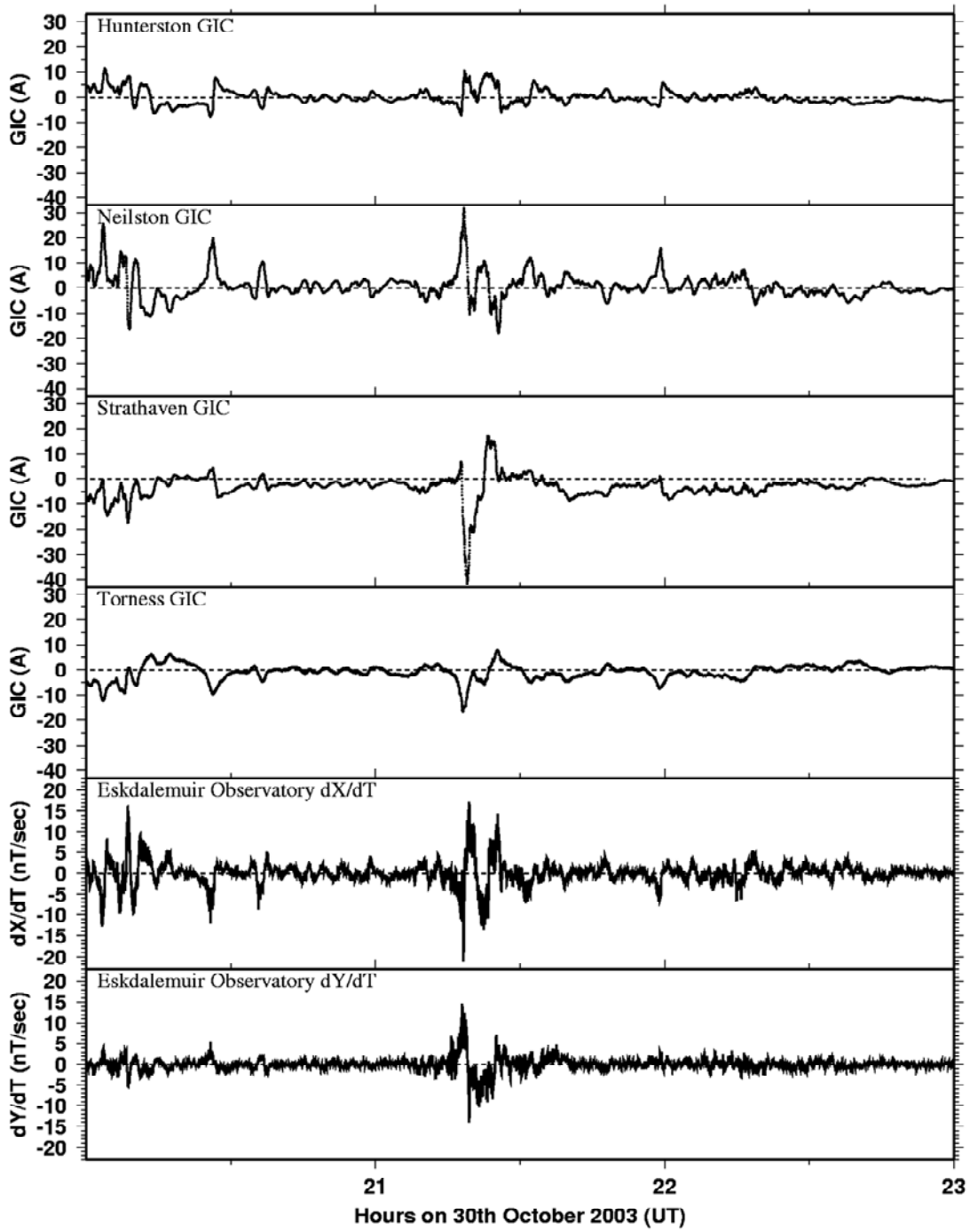

Figure 3. Measured GIC and field rates of change at Eskdalemuir for 30th October 2003. Data are shown at 1-second resolution. (Comparable data for the 29th October 2003 show numerous gaps in the GIC record.)

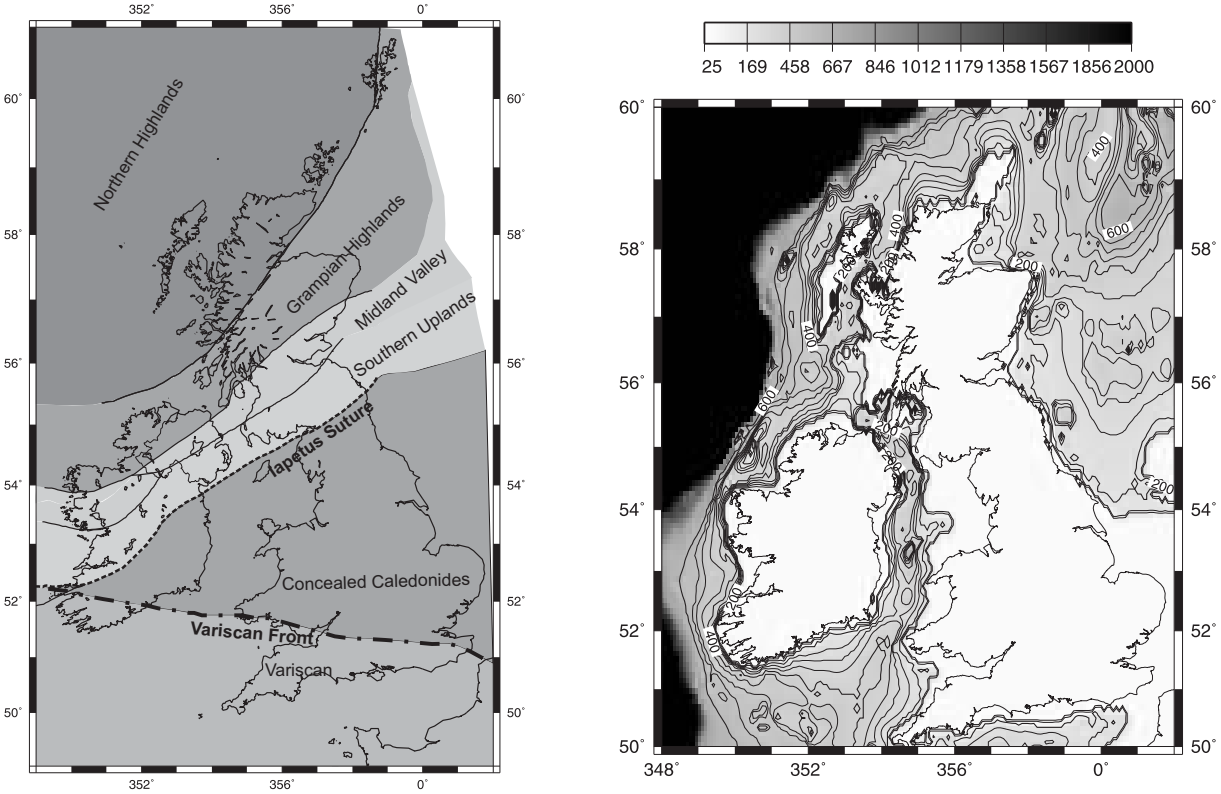

Figure 4. The tectonic structure of the British Isles (left) as simplified and used by Beamish *et al* (2002). The conductance (S) of the shelf seas and ocean is shown (right). This conductance is presented to the model as a thin surface layer atop the crustal model of Beamish *et al* (2002). For plotting purposes the maximum conductance has been limited to 2000S; in the deep Atlantic Ocean to the west the conductance reaches approximately15,000S. Onshore, the conductance of the thin sheet is 25S, except for a regional variation within the Midland Valley, Southern Uplands and the northern region of the Concealed Caledonides. Data taken from McKay (2004).

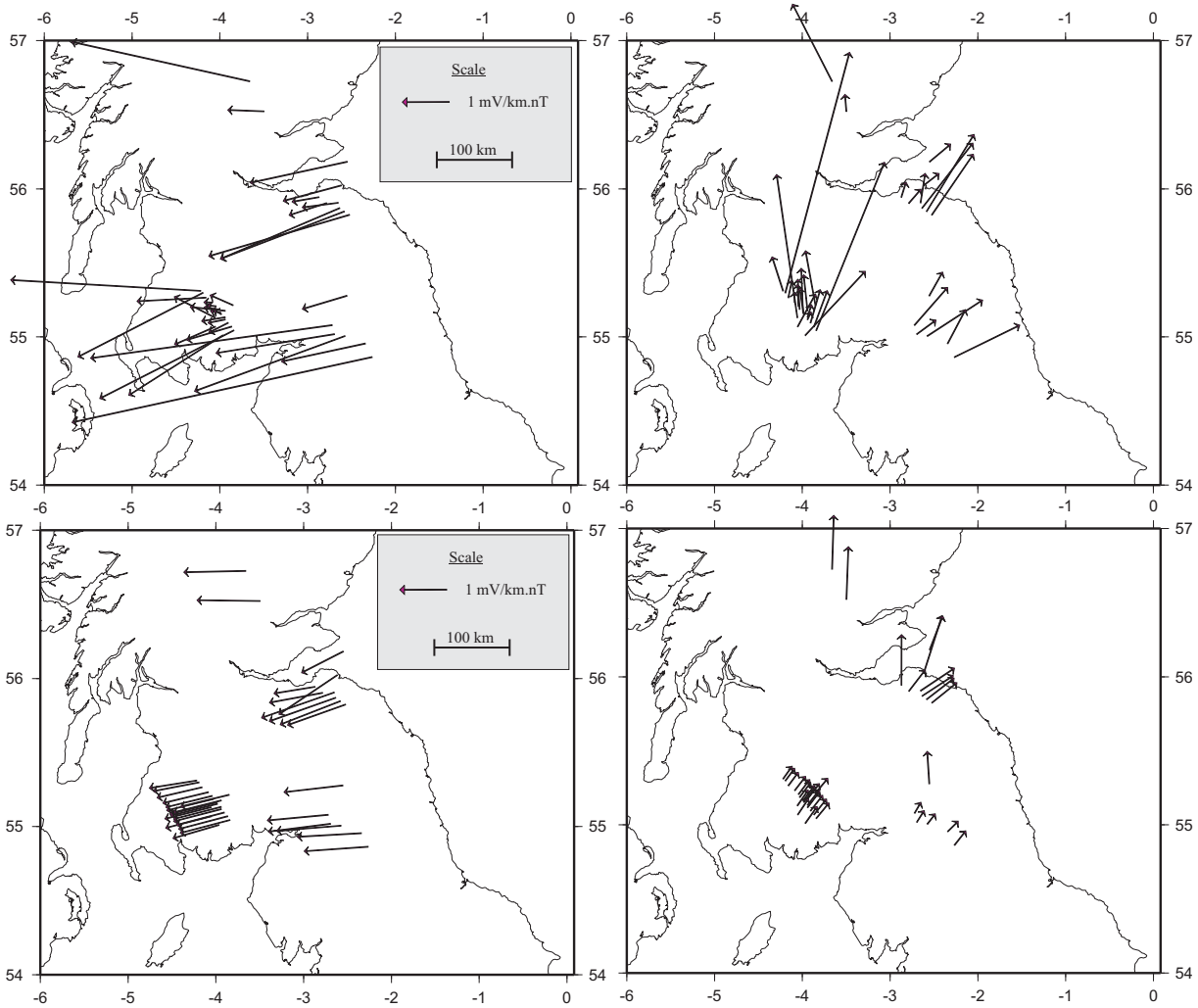

Figure 5. Telluric vectors of the scaled regional telluric response (top), from McKay (2004), at measurement sites across Scotland and Northern England. Model telluric vectors are shown below, for the same locations. Data on left (right) are for an east-west (north-south) inducing field.

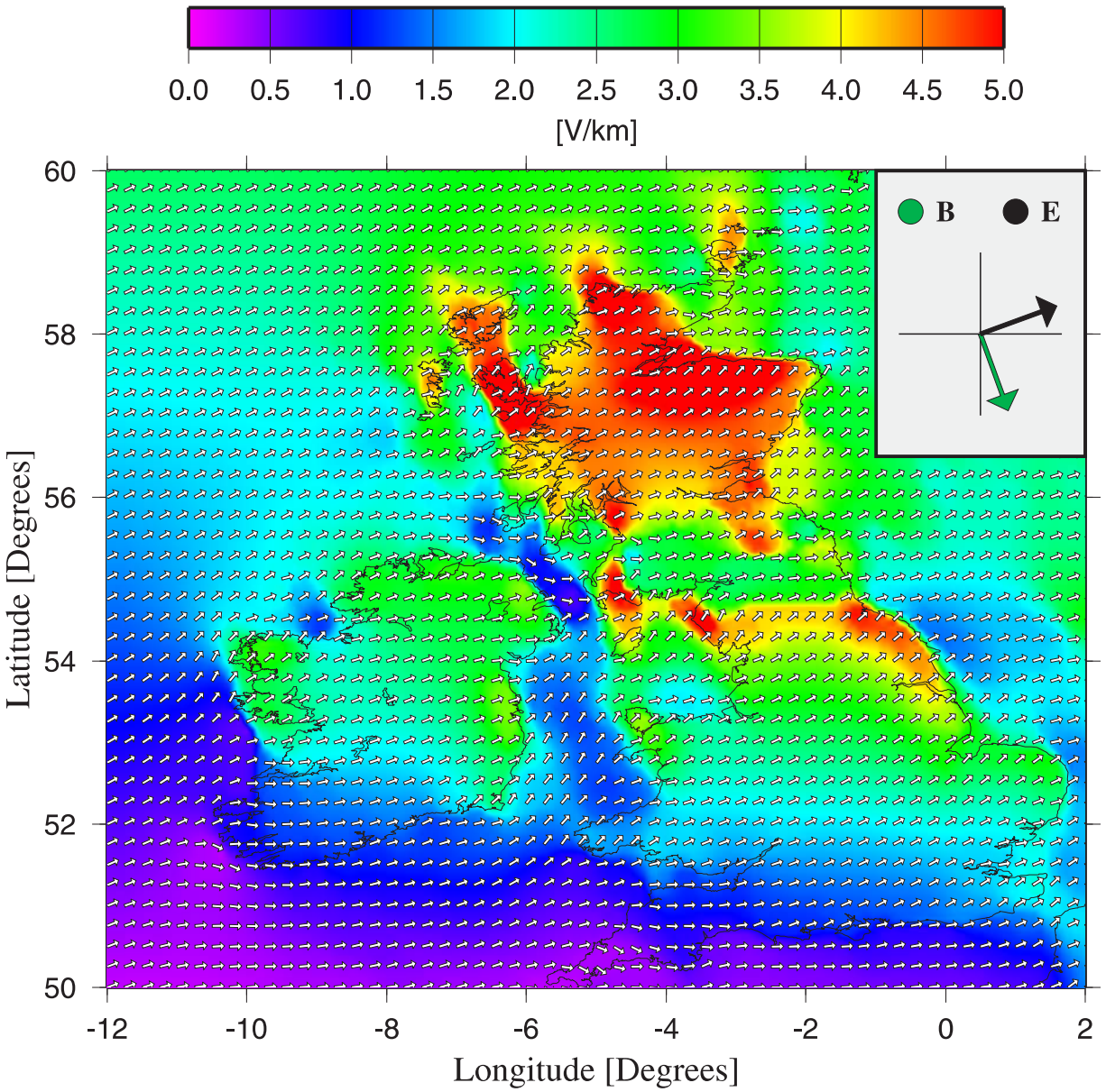

Figure 6. The surface electric field in the box shown in Figure 4 at 21:20 UT on 30th October 2003. Colour denotes *E*-field amplitude (see scale bar) in V/km. Small arrows denote the local field direction. The inset shows the regional *E*-field direction for a simpler 1D conductivity model, as well as the direction of the 360s period external magnetic field controlling induction at that time.

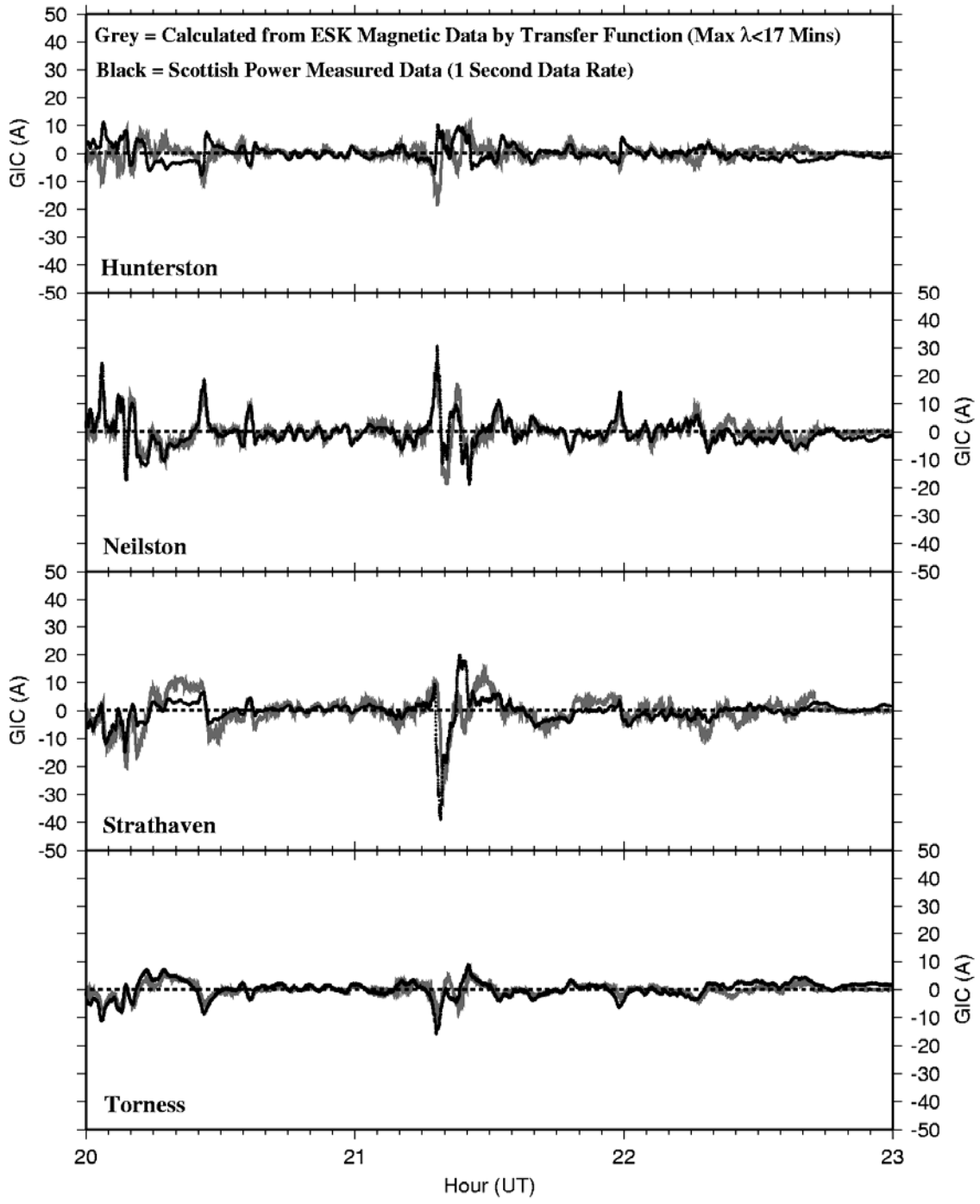

Figure 7. Transfer function model (gray lines) for the four permanent measurement sites, compared with measured data (black) for October 30th 2003. One-second measurements are used, with the longest transfer function wavelength less than about 17 minutes.

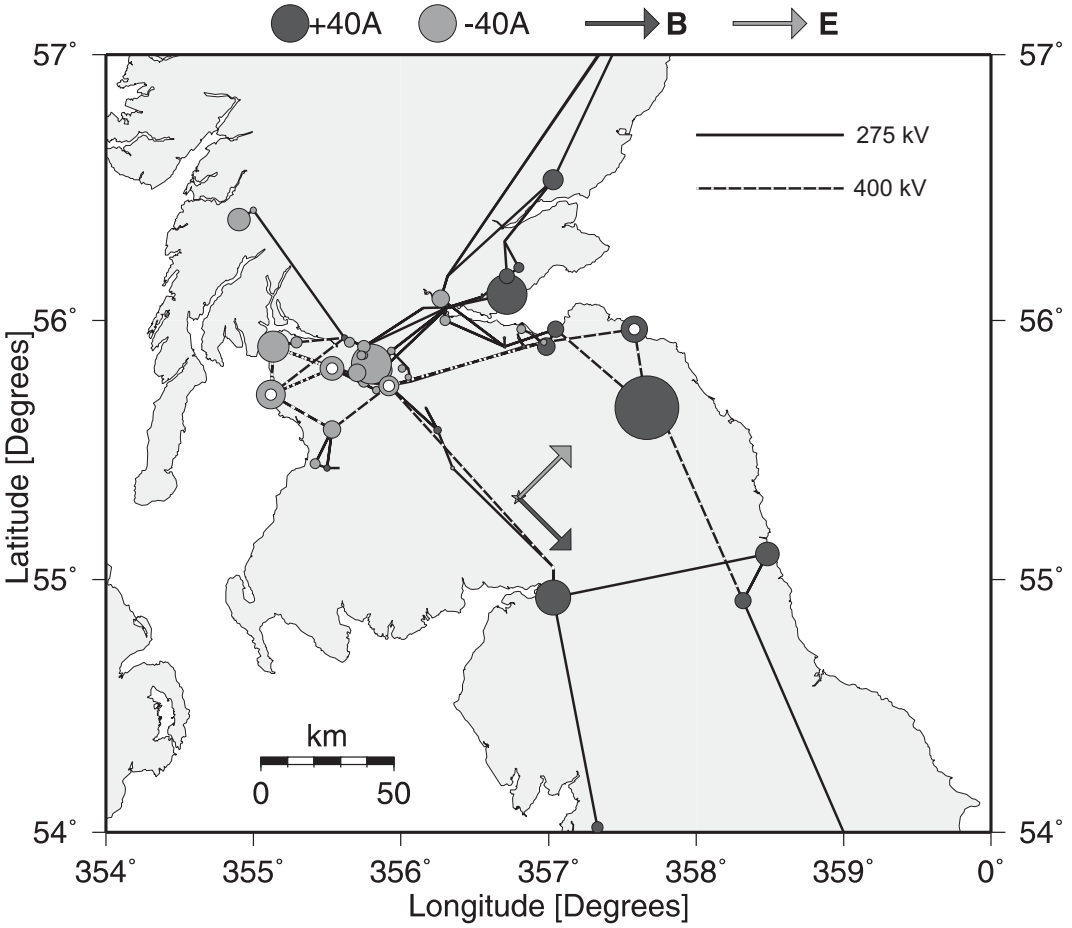

Figure 8. Estimated GIC from the grid network model of the Scottish Power grid, coupled with the surface electric field model of Figure 6 at the peak of the storm at 21:20 UT. Circle shade denotes GIC flowing to/from earth (dark/light) and the arrows denote the instantaneous field directions (*E*-field for a 1D conductivity model). Amplitudes are proportional to spot size, with 40A shown to scale. In order to show one value at each substation location the sum of all GIC at that site are given for clarity. White spots show the locations of the permanent GIC measurement sites.

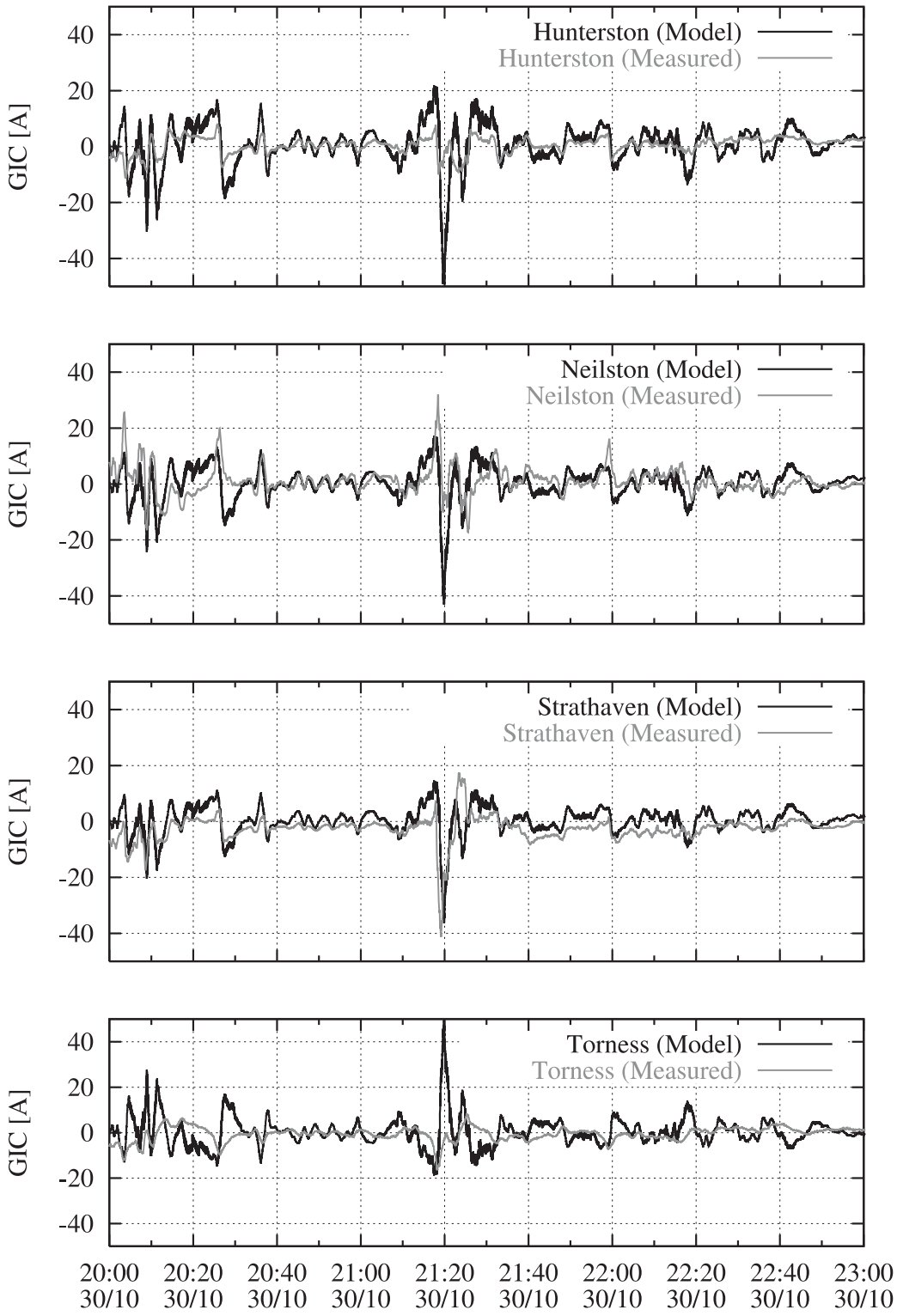

Figure 9. Time series of model and measured GIC at the Hunterston (HUNT), Neilston (NEIL) Strathaven (STHA) and Torness (TORN) sites between 20:00 UT and 23:00 UT on the 30th October 2003. Total site GIC model flows are shown.

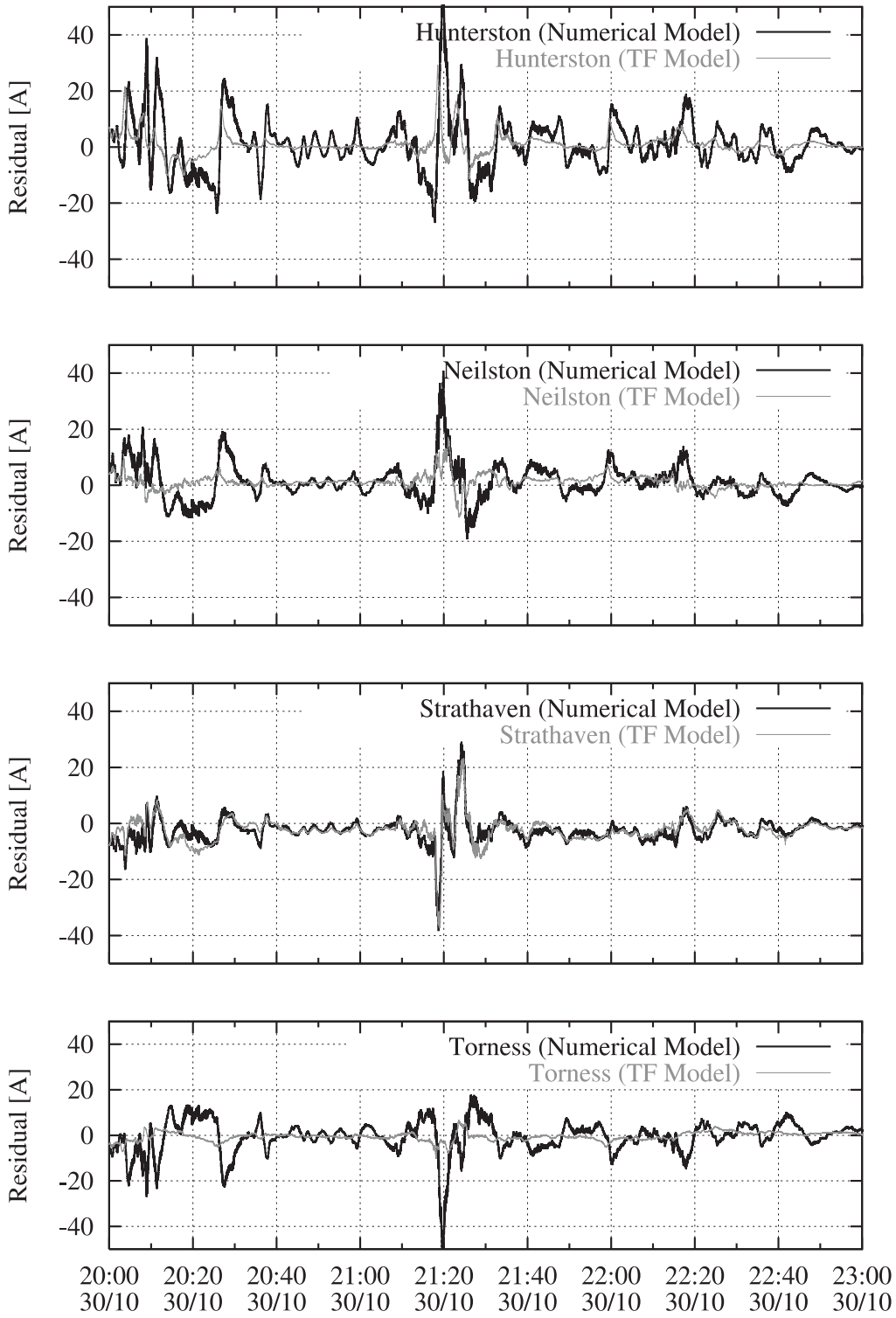

Figure 10. The point difference between GIC calculated using the numerical (black line) and transfer function (grey line) models between 20:00 UT and 23:00 UT on the 30th October 2003.

	P_{68} [A]	P_{95} [A]	P_{99} [A]	P_{95} [A]
HUNT	1.6	11.7	30.5	3.8
NEIL	1.1	7.5	19.2	3.1
STHA	3.0	6.7	23.4	7.1
TORN	1.4	8.5	26.0	3.0

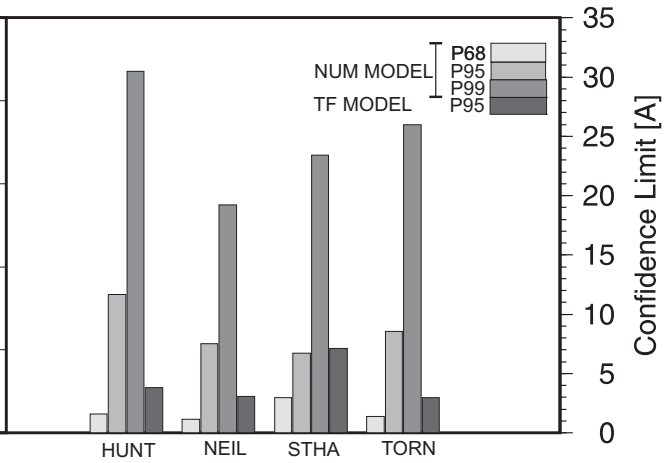

Figure 11. The GIC numerical (NUM) network model accuracy, based on quantile-quantile plots of residuals (in Amps) and shown at different levels of significance. Transfer function (TF) data are also given, for comparison, at the 95% confidence level in the fourth numerical column.

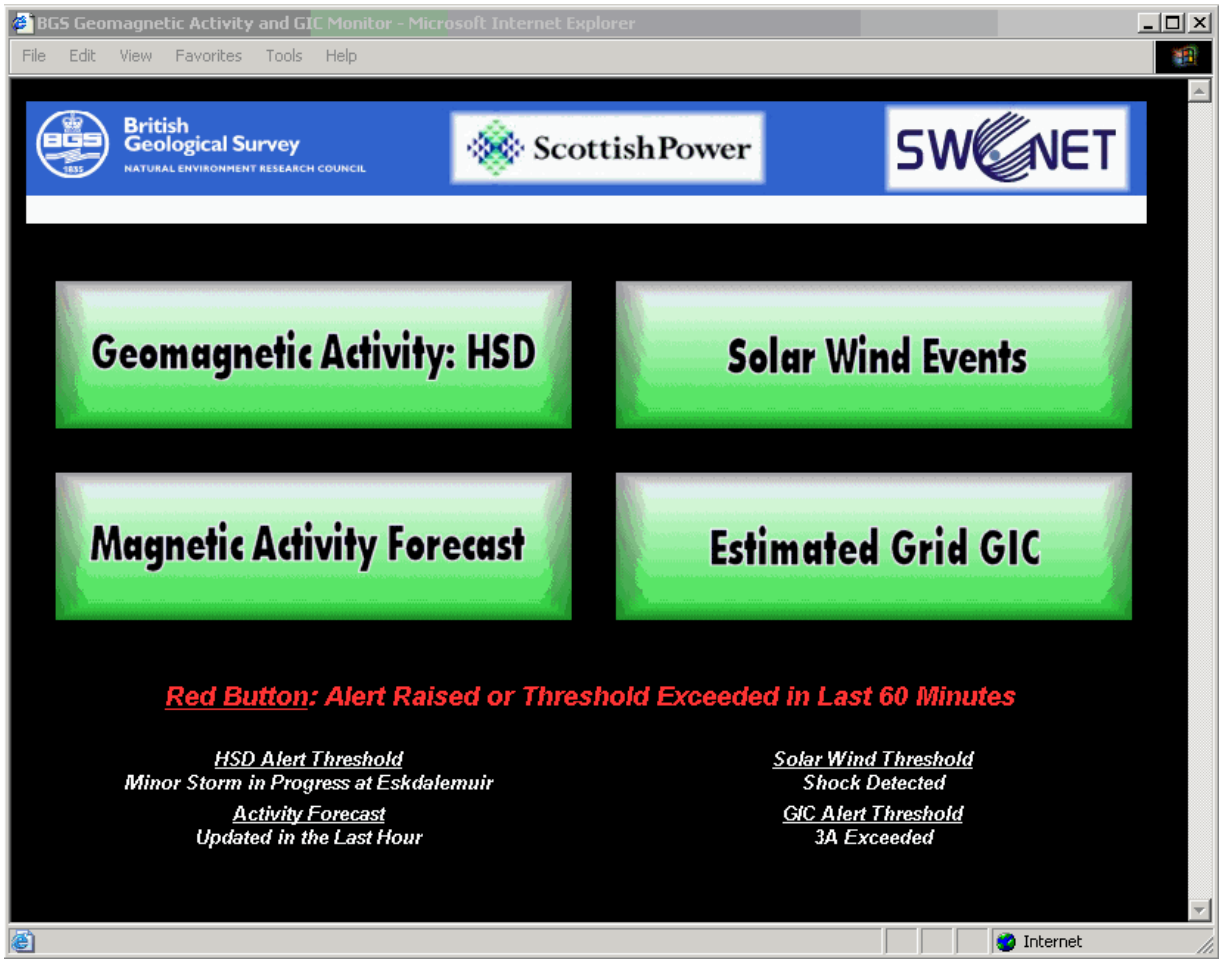

Figure 12. The front page of the web based data delivery system. The page is password protected.

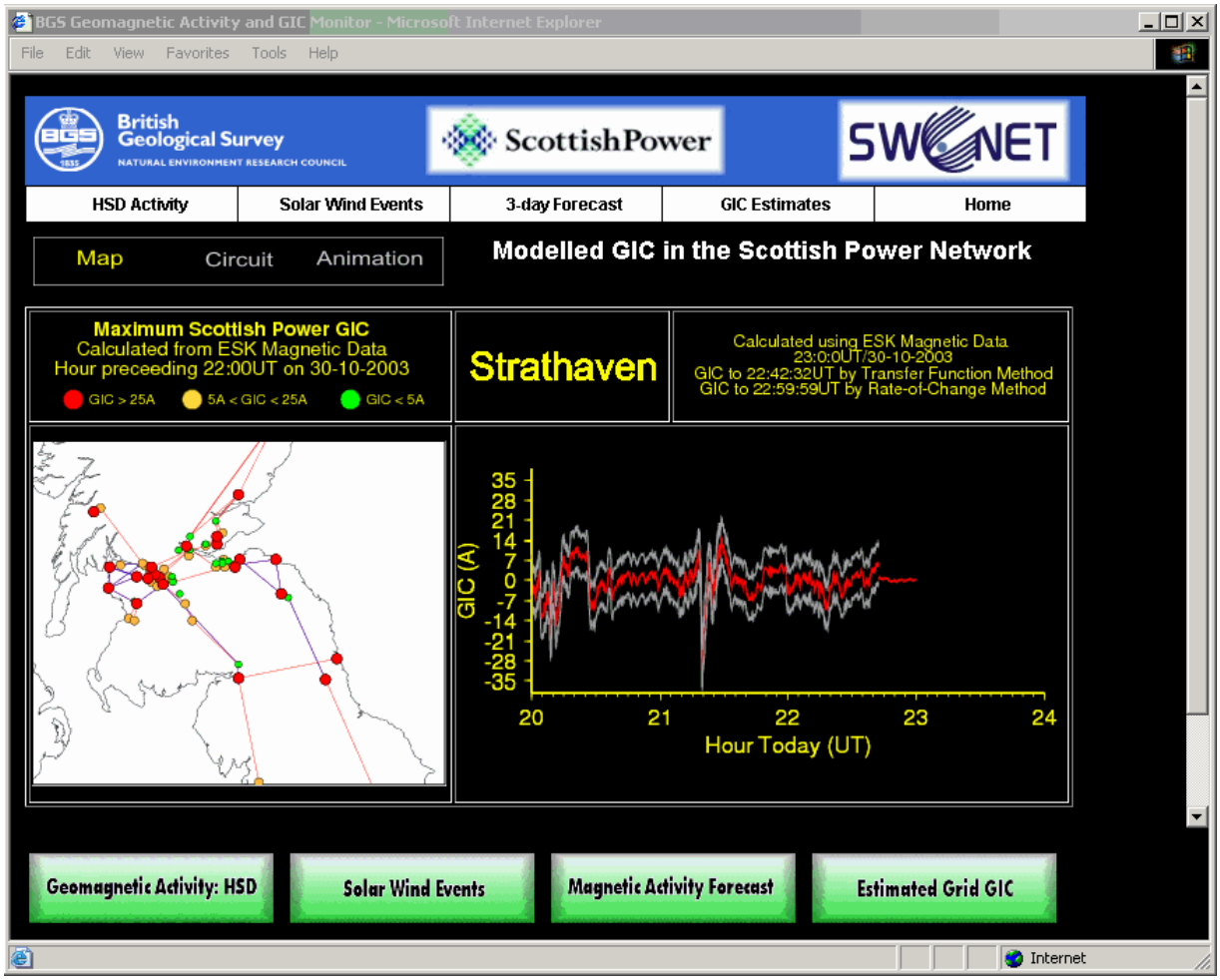

Figure 13. *Left*: Maximum GIC estimated in the grid in the hour prior to 22:00 UT on the 30th October 2003 (shown as a geographic map here rather than via the alternative option of a schematic layout of transformer earth points). *Right*: GIC time series for the four individual substations can be displayed, together with 95% confidence limits on the estimated current flow. The time series data are obtained from either the *E*-field and network model or (as here) from a transfer function model.